

**ARTICLE TYPE**

# Recognizing a Spatial Extreme dependence structure: A Deep Learning approach

Manaf AHMED<sup>1,2</sup> | Véronique MAUME-DESCHAMPS<sup>2</sup> | Pierre RIBEREAU<sup>2</sup>

<sup>1</sup>Department of statistics and Informatics,  
University of Mosul, Mosul, Iraq  
<sup>2</sup>Institut Camille Jordan, ICJ, Univ Lyon,  
Université Claude Bernard Lyon 1, CNRS  
UMR 5208, Villeurbanne, F-69622, France

**Correspondence**

Manaf AHMED,  
Email: manaf.ahmed@uomosul.edu.iq

**Summary**

Understanding the behaviour of environmental extreme events is crucial for evaluating economic losses, assessing risks, health care and many other aspects. In the spatial context, relevant for environmental events, the dependence structure plays a central role, as it influence joined extreme events and extrapolation on them. So that, recognising or at least having preliminary informations on patterns of these dependence structures is a valuable knowledge for understanding extreme events. In this study, we address the question of automatic recognition of spatial Asymptotic Dependence (AD) versus Asymptotic independence (AI), using Convolutional Neural Network (CNN). We have designed an architecture of Convolutional Neural Network to be an efficient classifier of the dependence structure. Upper and lower tail dependence measures are used to train the CNN. We have tested our methodology on simulated and real data sets: air temperature data at two meter over Iraq land and Rainfall data in the east cost of Australia.

**1 | INTRODUCTION**

Understanding extreme environmental events such as heat waves or heavy rains is still challenging. The dependence structure is one important element in this field. Multivariate extreme value theory (MEVT) is a good mathematical framework for modelling the dependence structure of extremes events (see for instance De Haan and Ferreira (2007) and Embrechts, Klüppelberg, and Mikosch (2013)). Max-stable processes consist in an extension of multivariate extreme value distributions to spatial processes and provide models for spatial extremes (see De Haan, Pereira, et al. (2006) and De Haan et al. (1984)). These max-stable processes are asymptotically dependent (AD). This may not be realistic in practice. Wadsworth and Tawn (2012) introduced inverted max-stable processes which are asymptotically independent (AI). Using AD versus AI models has important implications on the extrapolation of joined extreme events (see Bortot, Coles, and Tawn (2000) and Coles and Pauli (2002)). So that,

recognising the class of dependence structure is an important task when building models for environmental data. One of the main challenges is how to recognise the dependence structure pattern of a spatial process. Despite various studies dealt with spatial extremes models, we have not found works focused on the question of the automatic determination of AI versus AD for a spatial process. The usual approach is to use Partial Maximum Likelihood estimations after having chosen (from exploratory graph studies) a class of models. We propose a first deep learning approach to deal with this question. Many works using deep learning for spatial and spatio-temporal processes have been developed but none concerned with AD versus AI (see Wang, Cao, and Yu (2019)).

Artificial Intelligence techniques have demonstrated a significant efficiency in many applications, such as environment, risk management, image analysis and many others. We will focus on Convolutional Neural Network (CNN) which have ability in automatic extracting the spatial features hierarchically. It has been used e.g. on spatial dependencies from raw datasets. For instance, Zhu, Chen, Zhu, Duan, and Liu (2018) proposed a predictive deep convolutional neural network to predict the wind speed in a spatio-temporal context, where the spatial dependence between locations is captured. Liu et al. (2016) developed a CNN model to predict extremes of climate events, such as tropical cyclones, atmospheric rivers and weather fronts. Lin et al. (2018) presented an approach to forecast air quality (PM2.5 concentration) in a Spatio-temporal framework. While Zuo et al. (2015) improved the power of recognising objects in images by learning the spatial dependencies of these regions via CNN. In the spatial extreme context, Yu, Uy, and Dauwels (2016) tried to model the spatial extremes by bridging the gap between the traditional statistical method and Graph methods via decision Trees.

Our objective is to employ deep learning concepts in order to recognise patterns of spatial extremes dependence structures and distinguish between AI and AD. Upper and Lower tail dependence measures  $\chi$  and  $\bar{\chi}$  are used as a summary of the extreme dependence structure. These dependence measures have been introduced by Coles, Heffernan, and Tawn (1999) in order to quantify the pairwise dependence of extremes events between two locations. Definitions and properties of these measures will be given in Section 2. The pairwise empirical versions of these measures are used as a summary dataset. The CNN will be trained to recognise the pattern of dependence structures via this summary dataset.

Due to the influence of the air temperature at 2 meters above the surface on assessing climate changes and on all biotic processes, especially in extreme, we will apply our methods to this case study, data come from the European Center for Medium-Range Weather Forecasts ECMWF. The second case study is the rainfall amount recorded in the east coast of Australia.

The paper is organised as follows. Section 2 is devoted to the theoretical tools used in paper. An overview of Convolutional Neural Networks concepts is exposed in Section 3. Section 4 is devoted to configure the architecture of the CNN for classification of dependence structures. Section 5 shows the performance of our designed CNN on simulated data. Applications to environmental data: Air temperature and Rainfall events are presented in Section 6. Finally, a discussion and main conclusions of this study are given in Section 7.

## 2 | THEORETICAL TOOLS

Let us give a survey on spatial extreme models and tail dependence functions, see Coles et al. (1999) for more details.

### 2.1 | Spatial extreme models

Let  $\{X'_i(s)\}_{s \in S}$ ,  $S \in \mathbb{R}^d$ ,  $d \geq 1$  be i.i.d replications of a stationary process. Let  $a_n(s) > 0$  and  $b_n(s)$ ,  $n \in \mathbb{N}$  be two sequences of continuous functions. If

$$\left\{ \max_{i \in n} (X'_i(s) - b_n(s)/a_n(s)) \right\}_{s \in S} \xrightarrow{d} \{X(s)\}_{s \in S} \quad (1)$$

as  $n \rightarrow \infty$ , with non-degenerated marginals, then  $\{X(s)\}_{s \in S}$  is a max-stable process. Its marginals are Generalized Extreme Value (GEV). If for all  $n \in \mathbb{N}$ ,  $a_n(s) = 1$  and  $b_n(s) = 0$ , then  $\{X(s)\}_{s \in S}$  is called a simple max-stable process. It has unit Fréchet marginal, which means:  $\mathbb{P}\{X(s) \leq x\} = \exp(-1/x)$ ,  $x > 0$ , (see De Haan et al. (2006)). In De Haan et al. (1984), it is proved that any simple max-stable process defined on a compact set  $S \subset \mathbb{R}^d$ ,  $d \geq 1$  with continuous sample path admits a spectral representation as follows.

Let  $\{\xi_i, i \geq 1\}$  be an i.i.d Poisson point process on  $(0, \infty)$ , with intensity  $d\xi/\xi^2$  and let  $\{W_i^+(s)\}_{i \geq 1}$  be a i.i.d replicates of a positive random field  $W := \{W(s)\}_{s \in S}$ , such that  $\mathbb{E}[W(s)] = 1$ . Then

$$X(s) := \max_{i \geq 1} \{\xi_i W_i(s)^+\}, s \in S, S \in \mathbb{R}^d, d \geq 1 \quad (2)$$

is a simple max-stable process. The multivariate distribution function is given by

$$\mathbb{P}\{X(s_1) \leq x_1, \dots, X(s_d) \leq x_d\} = \exp(-V_d(x_1, \dots, x_d)), \quad (3)$$

where  $s_1, \dots, s_d \subset S$  and  $V$  is called the exponent measure. It is homogeneous of order  $-1$  and has the expression:

$$V_d(x_1, \dots, x_d) = \mathbb{E} \left[ \max_{j=1, \dots, d} \{W(s_j)/x_j\} \right], \quad (4)$$

The extremal dependence coefficient is given by  $\Theta_d = V_d(1, \dots, 1) \in [1, d]$ . It has been shown by Schlather and Tawn (2003) that for max-stable processes, either  $\Theta_d = 1$  which means that the process is asymptotically dependent (AD) or  $\Theta_d = d$  which is the independent case. If  $\Theta \neq 1$ , the process is said to be asymptotically independent (AI). For max-stable processes, AI implies independence. Wadsworth and Tawn (2012) introduced inverted max-stable processes which may be AI without being independent. Let  $\{X(s)\}_{s \in S}$  be a simple max-stable process, an inverted max-stable process  $Y$  is defined as

$$Y(s) = -1/\log\{1 - \exp(-1/X(s))\}, s \in S. \quad (5)$$

It has unit Fréchet marginal laws and its multivariate survivor function is

$$\mathbb{P}r\{Y(s_1) > y_1, \dots, Y(s_d) > y_d\} = \exp(-V_d(y_1, \dots, y_d)). \quad (6)$$

In the definition of max-stable processes, different models for  $W$  lead to different simple max-stable models, as well as inverted max-stable models. For instance, the Brown-Resnick model is constructed with  $W_i(s) = \{\epsilon_i(s) - \gamma(s)\}_{i \geq 1}$ , where  $\epsilon_i(s)$  are i.i.d replicates of a stationary Gaussian process with zero mean and variogram  $\gamma(s)$  (see Brown and Resnick (1977) and Kabluchko, Schlather, De Haan, et al. (2009)). Many other models have been introduced, such as Smith, Schlather and Extremal-t introduced respectively by Smith (1990), Schlather (2002) and Opitz (2013).

In what follows, we shall consider extreme Gaussian processes which are Gaussian processes whose marginals have been turned to a unite Fréchet distribution. We shall also consider max-mixture processes which are  $\max(aX(s), (1-a)Y(s))$  where  $a \in [0, 1]$ ,  $X(s)$  is a max-stable process and  $Y(s)$  is an invertible max-stable process or an extreme Gaussian process.

## 2.2 | Extremal dependence measures

Consider a stationary spatial process  $X := \{X(s)\}_{s \in \mathcal{S}}$ ,  $\mathcal{S} \subset \mathbb{R}^d$ ,  $d \geq 2$ . The upper and lower tail dependence functions have been constructed in order to quantify the strength of AD and AI respectively. The upper tail dependence coefficient  $\chi$  is introduced in Ledford and Tawn (1996) and defined by

$$\chi(h) = \lim_{u \rightarrow 1} \mathbb{P}(F(X(s)) > u | F(X(s+h)) > u), \quad (7)$$

where  $F$  is the marginal distribution function of  $X$ . If  $\chi(h) = 0$ , the pair  $(X(s+h), X(s))$  is asymptotically independent (AI). If  $\chi(h) \neq 0$ , the pair  $(X(s+h), X(s))$  is asymptotically dependent (AD). The process is AI (resp. AD) if  $\exists h \in \mathcal{S}$  such that  $\chi(h) = 0$  (resp.  $\forall h \in \mathcal{S}$ ,  $\chi(h) \neq 0$ ). In Coles et al. (1999), the lower tail dependence coefficient  $\bar{\chi}(h)$  is proposed in order to study the strength of dependence in AI cases. It is defined as:

$$\bar{\chi}(h) = \lim_{u \rightarrow 1} \left[ \frac{2 \log \mathbb{P}(F(X(s)) > u)}{\log \mathbb{P}(F(X(s)) > u, F(X(s+h)) > u)} - 1 \right], \quad 0 \leq u \leq 1. \quad (8)$$

We have  $-1 \leq \bar{\chi}(h) \leq 1$  and the spatial process is AD if  $\exists h \in \mathcal{S}$  such that  $\bar{\chi}(h) = 1$ . Otherwise, it is a AI.

Of course, working on data require to have empirical versions of these extreme dependence measures. We denote them respectively by  $\hat{\chi}$  and  $\hat{\bar{\chi}}$ , they have been defined in Wadsworth and Tawn (2012), see also Bacro, Gaetan, and Toulemonde (2016). Consider  $X_i, i = 1, 2, \dots, N$  the copies of a spatial process  $X$ , the corresponding empirical versions of  $\chi(h)$  and  $\bar{\chi}(h)$  are respectively

$$\hat{\chi}(s, t) = 2 - \frac{\log \left( N^{-1} \sum_{i=1}^N \mathbb{1}_{\{\hat{U}_i(s) < u, \hat{U}_i(t) < u\}} \right)}{\log \left( N^{-1} \sum_{i=1}^N \mathbb{1}_{\{\hat{U}_i(s) < u\}} \right)}, \quad (9)$$

and

$$\hat{\chi}(s, t) = \frac{2 \log \left( N^{-1} \sum_{i=1}^N \mathbb{1}_{\{\hat{U}_i(s) > u\}} \right)}{\log \left( N^{-1} \sum_{i=1}^N \mathbb{1}_{\{\hat{U}_i(s) > u, \hat{U}_i(t) > u\}} \right)} - 1, \quad (10)$$

where  $\hat{U}_i := \hat{F}(x_i) = N^{-1} \sum_{i=1}^N \mathbb{1}_{\{X \leq x_i\}}$ , for  $|s - t| = h$ .

### 3 | CONVOLUTIONAL NEURAL NETWORK (CNN)

A Convolutional Neural Network CNN is an algorithm constructed and perfected to be one of the primary branches in deep learning. We shall use this method in order to recognise the dependence structure in spatial patterns. It stems from two studies introduced by Hubel and Wiesel (1968) and Fukushima (1980). CNN are used in many domains, one of the common use is for image analysis. It appears to be relevant in order to identify the dependencies between nearby pixels (locations). It may recognise spatial features (see Wang et al. (2019)). Mainly, a convolutional neural network consists in three basic layers: Convolutional, pooling, and fully connected. The first two layers are dedicated to feature learning and the latter one for classification. Many researches present the CNN architecture, see e.g. Yamashita, Nishio, Do, and Togashi (2018) or Caterini and Chang (2018) for a mathematical framework. We shall not provide the details of the CNN architecture, as it exists in many articles and books, we refer the interested reader to the above references. Let us just recall that, reconsidering spatial data, a convolution step is required. It is helpful to make the procedure invariant by translation.

Once the CNN is build, the kernel values of the convolutional layers and the weights of the fully connected layers are learned during a training process.

Training is the process of adjusting values of the kernels and weights using known categorical datasets. The process has two steps, the first one is the forward propagation and the second step is the backpropagation. In forward propagation, the network performance is evaluated by a loss function according to the kernels and weights updated in the previous step. From the value of the loss, the kernel and weights is updated by a gradient descent optimisation algorithm. If the difference between the true and predicted class of the dataset is acceptable, the process of training stops. So that, selecting the suitable loss function and gradient descent optimisation algorithm is decisive for the quality of the constructed network performance. Determining the loss function (objective function) should be done according to the network task. Since our goal consists in classification, we shall use the cross-entropy as an objective function to minimize. Let  $y_a, a = 1, \dots, A$  be the true class (label) of the dataset and let  $\rho_a$  be the estimated probability of the  $a$ -th class, the cross-entropy loss function can be formulated as

$$L = - \sum_{a=1}^A y_a \log(\rho_a).$$

Minimizing the loss means updating the parameters, i.e. kernels and weights until the CNN predicts the correct class. This update will be done by the gradient descent optimization algorithm in the back propagation step. Many gradient algorithms

are proposed. The most commonly used in CNN are stochastic gradient descent (SGD) and Adam algorithm Kingma and Ba (2014). This algorithm is also an hyper-parameter in the network. To begin the training process, the data is divided into three parts. The first part is devoted to training CNN. Monitoring the model performance, hyperparameter tuning and model selection are done with the second part. This part is called validation dataset. This third part is used for the evaluation of the final model performance. This latter part of data has never been seen before by the CNN.

## 4 | CONFIGURE CNN TO CLASSIFY THE TYPES OF DEPENDENCE STRUCTURES

We shall now explain how we used the CNN technology for our purpose to distinguish extreme dependence structures in spatial data.

### 4.1 | Constructing the dependence structures of the event

Spatial extreme models may have different dependence structures, such as asymptotic dependence or asymptotic independence. These structures may be identified by many measures. The well known measures able to capture these structures are e.g. upper and lower dependence measures  $\chi$  and  $\bar{\chi}$  in Equations (7) and (8), respectively. Upper tail is able to capture the dependence structure for asymptotic dependence models, but it fails with asymptotically independent models. The lower tail measure treats this problem by providing the dependence strength for asymptotically independent models. We propose to consider these two measures  $\chi$  and  $\bar{\chi}$  as learning data for the CNN, because each of them provide information on each type of dependence structure. The empirical counterparts  $\hat{\chi}(h)$  and  $\hat{\bar{\chi}}(h)$  in Equations (9) and (10) respectively, computed above a threshold  $u$  will be used on the raw data to construct raster dataset with a symmetric array in two tensors, the first one for  $\hat{\chi}$  and the second for  $\hat{\bar{\chi}}$ . This array will present the dependence structure of the corresponding data. Figure 1 shows of an array constructed from Brown-Resnick and inverse Brown-Resnick models.

### 4.2 | Building CNN architecture

It is essential in the convolutional neural network design to take into account the kind of data and the task to be done: classification, representations, or anomaly detection. Practically, designing a CNN for classification of complex patterns remains challenging. First of all, one has to determine the number of convolutional and fully connected layers that should be used. Secondly, tuning a high number of parameters (kernel, weights) is required. Many articles are devoted to build and improve CNN architectures to have good performance: LeCun et al. (1990), Alex, Sutskever, and Hinton (2012), He, Zhang, Ren, and Sun (2016) and Xie, Girshick, Dollár, Tu, and He (2017).

These CNN architectures are appropriate for image classifications but not for our goal because we need to keep the dependence

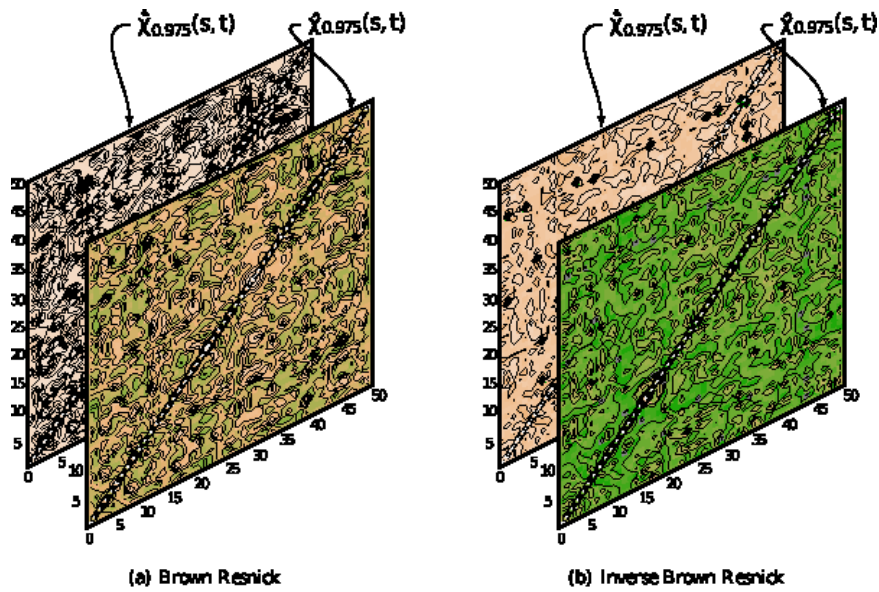


**FIGURE 1** Spatial dependence structures (layers) of data samples generated from: (a) Brown-Resnick - asymptotic dependent model ; (b) inverted Brown-Resnick - asymptotic independent model. The two models are generated with scale and smooth parameters 0.4 and 0.7, respectively. Two tensors are the empirical upper tail dependence measure  $\hat{\chi}_{0.975}(s, t)$  and the empirical lower tail dependence measure  $\hat{\chi}_{0.025}(s, t)$ ,  $s, t = 1, \dots, 50$ , respectively.

structure. So that, we designed a CNN for our dependence classification aim. From many attempts, we found out that quite a high number of parameters is required: not less than 17 million parameters. Figure 2 shows the general framework of the CNN architecture designed for the dependence classification.

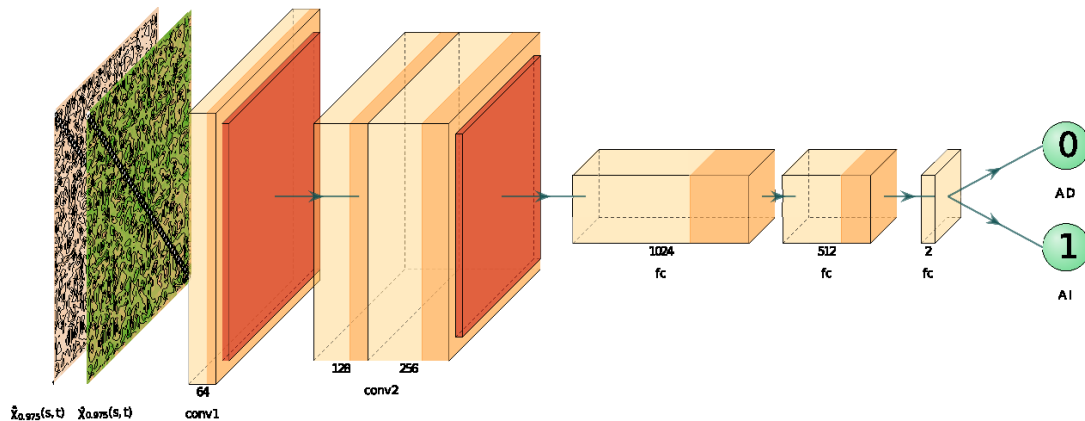


**FIGURE 2** CNN architecture designed for classification asymptotic dependence and asymptotic independence models. The input data is the dependence structure array with two tensors, one for  $\hat{\chi}_{0.975}(s, t)$  and the second for  $\hat{\chi}_{0.025}(s, t)$ . Three convolutional layers with two max-pooling and fully connected layers are the main parts of the CNN. The third layer is devoted to classification.

The Input of this designed CNN is the dependence structure layers, consisting in two tensors, one represents  $\hat{\chi}(s, t)$  and the other one represents  $\hat{\chi}(s, t)$ , where  $s, t = 1, \dots, 50$ .

Two networks are constructed, one has two classes output called 2-class, for recognizing asymptotic dependence vs asymptotic independence dependence structure. The second CNN has a third output class in order to detect if a spatial process is neither AD nor AI. The third class is considered as unknown dependence structure type. Table 1, shows the details of the architectures.

**TABLE 1** Designed Convolution Neural Network architecture for the two classes output. For the CNN with three output classes, the architecture is the same but the last fully connected layer has three units rather than two.

Layer type	Feature Map	Size of Kernels	Stride size	Padding	Activation
Input	–	–	–	–	–
2D-Convolutional	64	$3 \times 3$	$2 \times 2$	Valid	ReLU
2D-Max Pooling	–	$2 \times 2$	$1 \times 1$	Valid	–
2D-Convolutional	128	$3 \times 3$	$1 \times 1$	Valid	ReLU
2D-Convolutional	256	$3 \times 3$	$1 \times 1$	Valid	ReLU
2D-Max Pooling	–	$2 \times 2$	$1 \times 1$	Valid	–
Fully Connected	1024	–	–	–	ReLU
Fully Connected	512	–	–	–	ReLU
Output	2	–	–	–	Softmax

A regularizer with regularization factor  $l_2 = 0.00005$  is added to each convolutional layer. The gradient rate is set to be  $\alpha = 0.0001$  when updating the weights of the model. The total parameters for this architecture is more than 17 million and 45 million for datasets with 30 and 40 locations, respectively. In deep learning, the choice of an optimization algorithm is crucial in order to reach good results. Adam optimization algorithm is very effective with CNN (see Kingma and Ba (2014)). In this study, Adam optimization algorithm with a learning rate  $\lambda = 0.0001$  has been used. Since the dataset are categorical, the cross-entropy objective function is more suitable. Keras package in R interface is used for model learning.

## 5 | EVALUATION OF THE PERFORMANCE OF CNN VIA SIMULATION

In order to evaluate the performance of the constructed CNN networks in the previous section, three scenarios have been applied. For each scenario, the 2-class and 3-class networks are trained on AD and AI processes, for the 3 class networks, max-mixture processes (see definition in Section 2.1) are added to the training data. Our training data consists in:

- max-stable processes (defined in Equation (2)) with 1000 observations on sites  $s_i$ ,  $i = 1, \dots, 30$ , 60000 datasets are generated from four spatial extreme models: Smith, Schather, Brown-Resnick and Extremal-t with scale and smooth parameters  $\sigma$  and  $\delta$  respectively. These parameters are either chosen at random or in regular sequences,
- inverse max-stable as defined in (5) with the same parameters as above and 5000 datasets are generated from extreme Gaussian processes in order to have more variety in AI models.



In total, for the two dependence structure types 125000 datasets are generated and divided into three parts, 64% for training, 16% for validation and 20% for testing. Empirical  $\hat{\chi}_{0.975}(s_i, t_i)$  and  $\hat{\chi}_{0.975}(s_i, t_i)$  with  $(s_i, t_i) \in [0, 1], i = 1, \dots, 30$  defined in (9) and (10) respectively are used to summarize the datasets and are the inputs for training the CNN. For the 3-class network, we added 12000 datasets with neither AD nor AI dependence structure, through max-mixture processes. We have performed several scenarios.

- In the first scenario, for each dataset, the locations  $s \in [0, 1]^2$  are uniformly randomly chosen. Moreover the scale and smoothness parameters are also uniformly randomly selected:  $\sigma \sim U(0, 1)$  and  $\delta \sim U(1, 1.9)$ . In the 3-class network, the mixing parameter  $a$  is also uniformly randomly selected:  $a \sim U(0, 1)$ . The AD and AI models in the max-mixture are also chosen at random in the different classes.
- In the second scenario, the locations was fixed for all datasets, and the parameters remain chosen at random.
- In the third scenario, the locations are fixed for all datasets and the parameters ran through regular sequences,  $\sigma \in [0.1, 1]$  and  $\delta \in [0.1, 1.9]$ , with steps 0.2, the mixing parameter  $a \in [0.3, 0.7]$  with steps 0.1.

The evaluation task is done for the three scenarios described above. The datasets used are AD or AI for the 2-class networks and we added max-mixture processes for the 3-class networks. For the random scenarios, the evaluation datasets sites and parameters are chosen at random. For the fix locations scenario, evaluation datasets sites are chosen different from the training ones. For scenario 3, scale and smoothness parameters are chosen different for evaluation and training. The losses and accuracy for all datasets considered for the evaluation are shown in Table 2 .

**TABLE 2** The losses and Accuracy of 2-class and 3-class CNN networks trained within the three scenarios.

	Scenario 1 Fixed locations and random parameters				Scenario 2 Random locations and random parameters				Scenario 3 Fixed locations and sequential parameters			
	2-class Network		3-class Network		2-class Network		3-class Network		2-class Network		3-class Network	
	Loss	Accuracy	Loss	Accuracy	Loss	Accuracy	Loss	Accuracy	Loss	Accuracy	Loss	Accuracy
Training	0.3255	0.8668	0.6829	0.7232	0.3649	0.8386	0.3740	0.8749	0.2985	0.8824	0.4729	0.8242
validation	0.3525	0.8564	0.7071	0.7108	0.3675	0.8406	0.4763	0.8411	0.3285	0.8658	0.5204	0.8018
testing	0.3582	0.8547	0.7080	0.7146	0.3694	0.8400	0.5165	0.8039	0.3275	0.8672	0.5169	0.8041
Gaussian	0.0700	0.9969	0.0928	1.0000	0.2851	0.9550	0.3868	0.9540	0.0658	0.9980	0.0655	0.9980
Asymptotic dependent	0.4085	0.7880	0.7052	0.6870	0.4796	0.7050	0.6378	0.6660	0.3772	0.7940	0.5493	0.7480
Asymptotic independent	0.2889	0.9390	0.5124	0.8970	0.2753	0.9610	0.4621	0.9120	0.3284	0.9020	0.3317	0.9240
Mixtures	—	—	0.7437	0.6510	—	—	6.0335	0.1370	—	—	0.8299	0.6633
Different locations	0.779	0.8060	0.8888	0.8000	—	—	—	—	0.9536	0.8010	1.1231	0.7990
Different scale parameters	—	—	—	—	—	—	—	—	0.3908	0.8480	0.5024	0.8100
Different smooth parameters	—	—	—	—	—	—	—	—	0.3295	0.8744	0.4361	0.8355

The training progress is illustrated in Figure 3 .

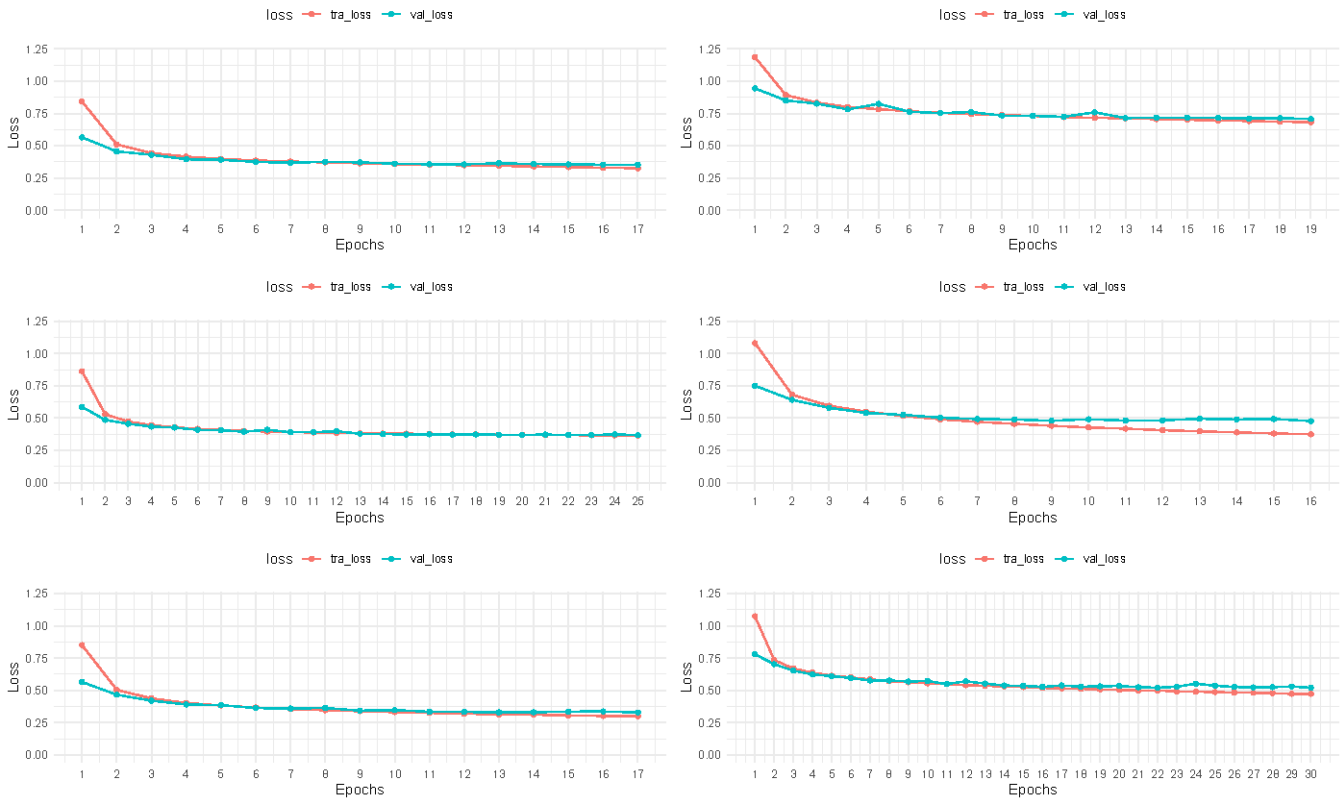


**FIGURE 3** Loss for training and validation for each scenario and class network. Each row represents the progress for scenarios 1,2 and 3, respectively. While the columns represent the process of the 2-class and 3-class networks, respectively.

Regarding the general performances of the scenarios illustrated in Figure 3 , the training progress of all networks is correct, the training and validation losses decrease, we observe no under nor overfitting and, moreover the procedure is stable. The network training will stop when there is no more improvement on the validation loss.

The first three rows of Table 2 show the training validation and testing losses. We can conclude that both 2-class and 3-class networks perform well for the 3 scenarios. The generalization is better with the third scenario. The performance of the networks may also be examined specifically for different dependence structures. Asymptotic independence structure (inverse max-stable or extreme Gaussian) is recognized almost perfectly by all networks as shown in the Table 2 . The performance in recognizing the asymptotic dependent structures is less satisfactory. The best results are obtained for Scenario 3, both for 2 and 3-class networks. The mixed dependence structure may be recognized by the 3-class networks: the second scenario failed to distinguish it, while the two other scenarios provide acceptable results. For the different location tests, the networks trained with scenario 1 overcome those trained with scenario 3. This is because the networks trained with random  $\sigma$  and  $\delta$  parameters lead to different dependence structures. In other words, no specific dependence structures are learned, contrary to the third scenario.

The performances are much improved by training the networks with datasets whose parameters cover sequences of parameters. Finally, scenario 3 has good performances, even for datasets with untrained scale and smooth parameters. These observations lead us to use the third scenario in our application studies: 2-meters air temperature over Iraq and the rainfall over the East coast of Australia.

## 6 | APPLICATION TO THE ENVIRONMENTAL CASE STUDIES

Modeling spatial extreme dependence structure on environmental data is our initial purpose in this work. We finish this paper with two specific studies on Iraqi air temperature and East Austrian rainfall.

### 6.1 | Spatial dependence pattern of the air temperature at two meter above Iraq land

Temperature of the air at two meters above the surface has a major influence on assessing climate changes as well as on all biotic processes. This data is inherently a spatio-temporal process (see Hooker, Duveiller, and Cescatti (2018)).

#### 6.1.1 | The data

We used data produced by the meteorological reanalysis ERA5 and achieved by the European Center for Medium-Range Weather Forecasts ECMWF. An overview and quality assessment of this data may be found in <http://dx.doi.org/10.24381/cds.adbb2d47>. Our objective is to study the spatial dependence structure pattern of this data recorded from a high temperature region in Iraq. Let  $\{X_k(s)\}_{s \in \mathcal{S}, k \in \mathcal{K}}$ ,  $\mathcal{S} \subset \mathbb{R}^2$ ,  $k \in \mathcal{K} \subset \mathbb{R}^+$ , be the daily average of the 2 meter air temperature process computed at the peak hours from 11H to 17H for the period 1979-2019 along of the summer (June, July and August). This collection of data results in  $|\mathcal{K}| = 3772$  temporal replications and  $|\mathcal{S}| = 1845$  grid cells. The data has naturally a spatio-temporal nature. Nevertheless, a preliminary preprocessing suggests us to treat them as independent replications of a stationary spatial process. The left panel in Figure 4 shows the time series of the  $X$  for three locations located in the north, middle and south of Iraq (white triangles on the right panel). The right panel, shows the temporal mean.

Regarding the time series in the left panel, the data in three locations may be considered as stationary in time. In order to remove the spatial non stationarity, we shall apply a simple moving average, as used in Huser (2020), see Section 6.1.2.

#### 6.1.2 | Preprocessing of 2 meter air temperature data.

As mentioned above, the 2 meter summer air temperature data in Iraq look spatially non stationary. We propose to follow Huser (2020), in order to remove the non stationarity. We shall decompose the spatial process  $\{X(s)\}_{s \in \mathcal{S}}$  into two terms, the average

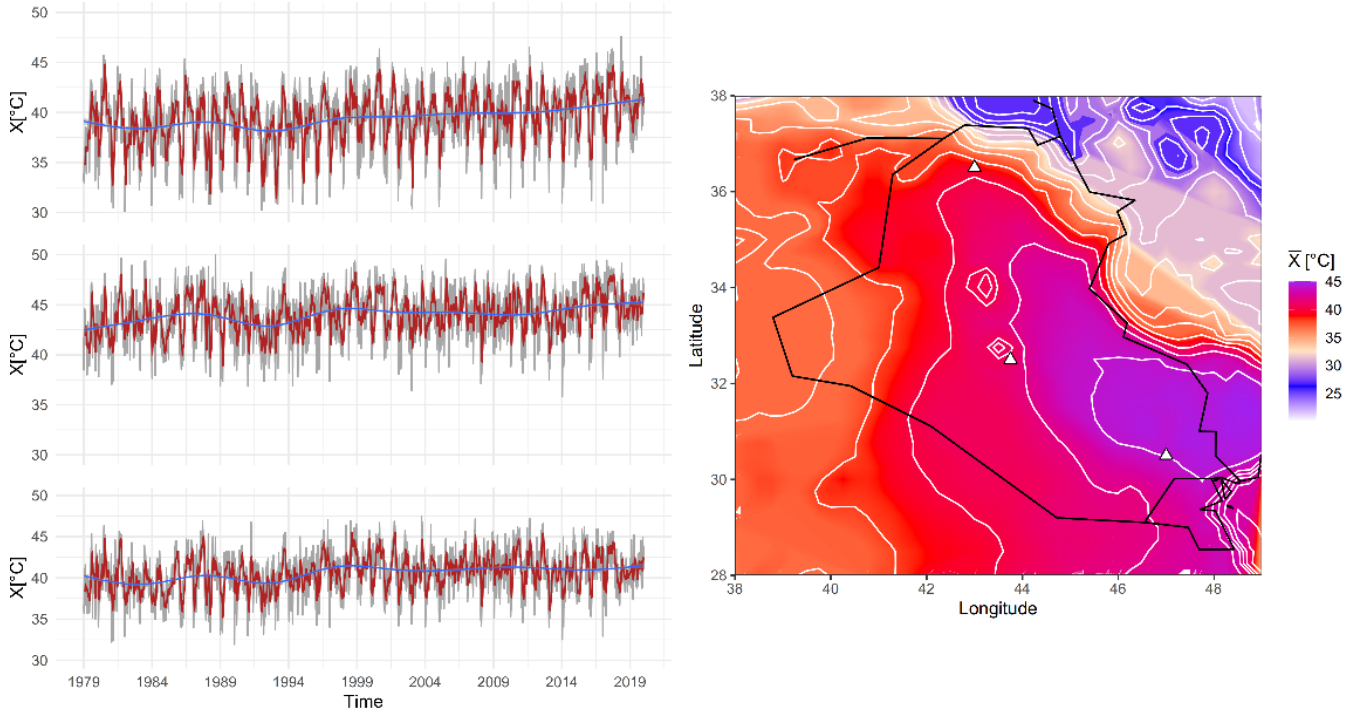


**FIGURE 4** Left panel, (gray lines) represent the time series of the daily average of the 2 meter air temperature for the period 1979-2019 verobalong summer months (June, July and August). The red lines represent the simple 10 days moving average. The smoothing temporal data is in blue line. The contour plot in the right panel shows the gradient level in the mean of  $X$  for the entire period above the Iraq land.

part  $\mu(s)$  and the residual part  $R(s)$ , so that

$$X(s) = \mu(s) + R(s). \quad (11)$$

Smoothing the empirical estimation of  $\mu_k(s)$  by a moving average over 10 days leads to

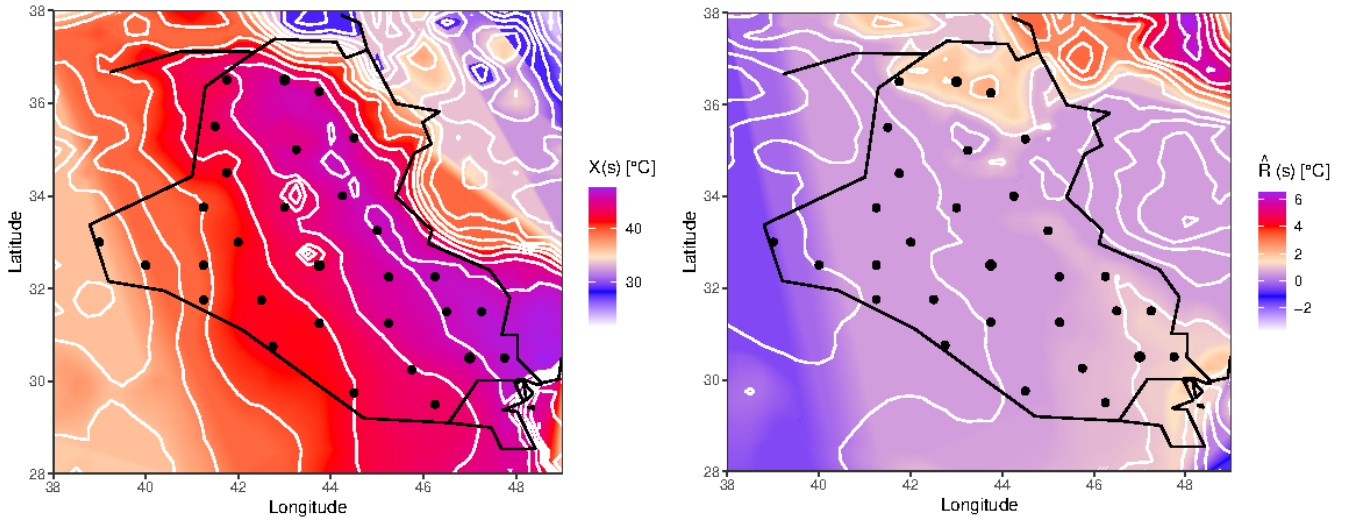
$$\hat{R}_k(s) = X_k(s) - \hat{\mu}_k(s), s \in S, k \in \mathcal{K}.$$

Figure 5 , shows the spatial variability for August, 15th 2019. One sees the non stationarity of  $(X_k(s))_{s \in S}$ , while the residuals  $\hat{R}_k(s)$  seem stationary (right panel).

In model (11), the residual process carries the dependence structure, we study below the isotropy of it. Figure 6 shows the estimated tail dependence functions with respect to some directions (where 0 is the north direction). From this graphical study, we may retain the istropy hypothesis.

We shall estimated the extremal dependence structure on block maxima. Let  $m \in \mathcal{K}$ ,  $k \in S$  and let

$$B_{m,k}(s) = \{(s, k) : (k - m) \leq k \leq (k + m)\} \cap (S \times \mathcal{K})$$



**FIGURE 5** Two meter air temperature  $X_k(s)$  over Iraq at August 15th, 2019 in the left panel, while the estimated residual process  $\hat{R}_k(s)$  is in the right panel. The black dots are the locations chosen to construct the air temperature dependence structure.

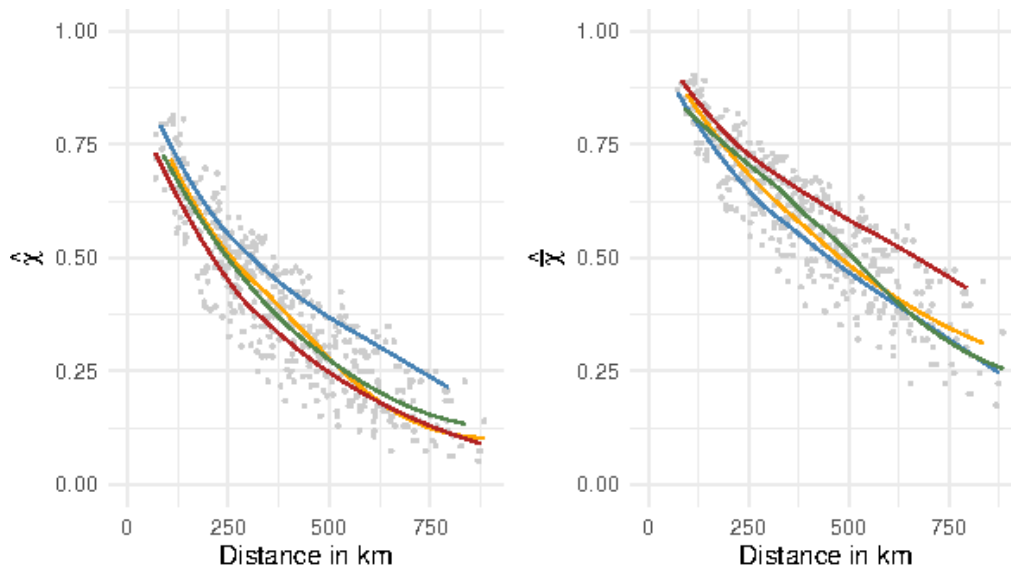


**FIGURE 6** Empirical tail dependence measures  $\hat{\chi}_{0.975}(h)$  and  $\hat{\lambda}_{0.975}(h)$ , for each direction. The red line is for direction  $(-\pi/8, \pi/8]$ , blue for  $(\pi/8, 3\pi/8]$ , green for  $(3\pi/8, 5\pi/8]$  and black for  $(5\pi/8, 7\pi/8]$ , where  $h = \|s - t\|, s, t \in S$ . The gray dots represent the pairwise  $\hat{\chi}_{0.975}(s, t)$  and  $\hat{\lambda}_{0.975}(s, t)$  for all dataset.

be a temporal neighborhood set of  $\hat{R}_k(s)$  for each grid cell  $s$ , the extreme spatial process is defined as

$$Y_k(s) = \max_{(s, k^*) \in \mathcal{B}_{m,k}(s)} \hat{R}_{k^*}(s).$$

Then, dependence structure of the air temperature will be estimated using  $\hat{\chi}_{0.975}(s, t)$  and  $\hat{\chi}_{0.975}(s, t)$ ,  $s, t = 1, \dots, 30, (s, t) \in S$ .

We shall consider the rank transformation applied on  $Y$ , in order to transform the margin to unite Fréchet:

$$\hat{Y}_k(s) = \begin{cases} -1/\log(\text{Rank}(Y_k(s))/(|\mathcal{B}_{m,k}(s)| + 1)) & \text{if } \text{Rank}(Y_k(s)) > 0 \\ 0 & \text{if } \text{Rank}(Y_k(s)) = 0, \end{cases}$$

where  $k = 1, \dots, |\mathcal{B}_{m,k}(s)|$ ,  $s = 1, \dots, 30$  and  $|\cdot|$  is the cardinality, we get a  $[30 \times 30 \times 2]$  table which will consists in the CNN inputs.

### 6.1.3 | Training the designed Convolutional Neural Network

We shall now use the CNN procedure described in Sections 4 and 5, we consider the locations of the data, according to scenario 3. We resize the data into  $[0, 1]^2$ . The training datasets are generated as in scenario 3, for parameters, we use regular sequences with steps 0.1. Figure 7, shows the loss of the training progress for the designed CNN 2-class network. The performance of the 3-class network is comparable.



**FIGURE 7** The loss of training and validation recorded for each of the 14 epochs during the training progress.

As we mentioned previously, the CNN will stop on training when the validation loss reaches the minimum. At the epoch 14, the training and validation loss recorded at 0.2282 and 0.2427 respectively, with accuracy 0.9333 and 0.9321 respectively. For testing data the loss was 0.2512 and accuracy 0.9260. This shows that the training process worked well.

### 6.1.4 | Predicting the dependence structure class for two meter summer air temperature

The prediction of the pattern of air temperature dependence structure is done according to 7 sizes of block maxima,  $m = 192, 30, 15, 7, 5, 3, 1$  which gives respectively 41, 125, 251, 538, 754, 1257 blocks from  $K = 3772$  measurements, so that we

shall see the influence of block size on the predicted class. Table 3 shows the predicted pattern of the dependence structure of 2 meter air temperature corresponding to each block maxima size proposed. For all block sizes, the predicted pattern was asymptotic dependence, with no significant effect of block size on the probability of prediction for both 2-class and 3-class CNN. So, we may conclude that the 2 meter air summer temperature has an asymptotic dependent spatial structure.

**TABLE 3** Predicted class and its probability for the 2 meter air temperature data for each block maxima size proposed. The dependence structure is validated by the two CNN. AD and AI refer to asymptotic dependence and asymptotic independence, respectively.

Block Maxima size	2 classes CNN		3 Classes CNN		
	Probability of AD	Probability of AI	Probability of AD	Probability of AI	Probability of mix
$m = 92$ days	1.000	0.000	1.000	0.000	0.000
$m = 30$ days	1.000	0.000	1.000	0.000	0.000
$m = 15$ days	0.990	0.001	0.645	0.355	0.000
$m = 7$ days	0.860	0.140	0.791	0.199	0.010
$m = 5$ days	0.929	0.071	0.686	0.013	0.301
$m = 3$ days	0.864	0.136	0.702	0.085	0.213
$m = 1$ day	0.995	0.005	0.950	0.037	0.013

## 6.2 | Rainfall dataset: case study in Australia

Another dependence structure investigated in this paper is the daily rainfall data recorded in 40 monitoring stations located in East of Australia illustrated by the red dots in Figure 8 . This dataset has been studied by several authors Abu-Awwad,

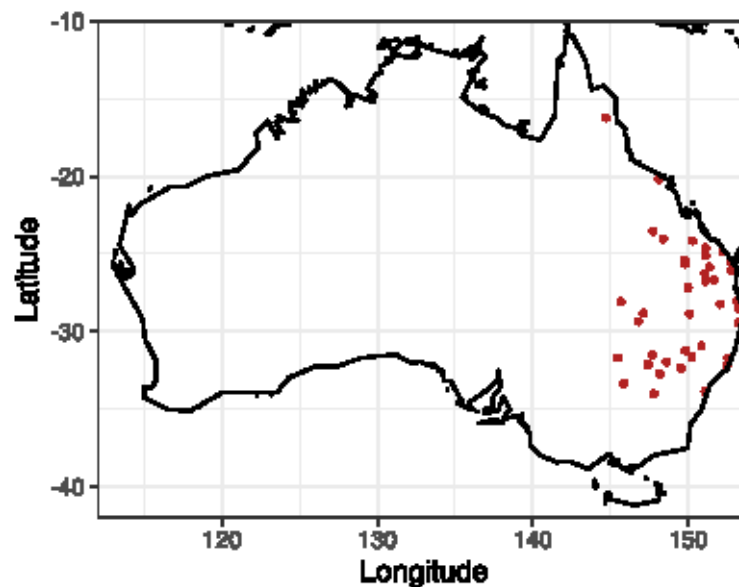


**FIGURE 8** Australia map illustrate the coordinates of rainfall monitoring stations.



Maume-Deschamps, and Ribereau (2019); Ahmed, Maume-Deschamps, Ribereau, and Vial (2017); Bacro et al. (2016).

### 6.2.1 | The data

For each location, the cumulative rainfall amount (in millimeters) over 24 hours is recorded, during the period 1972-2019 along the extended rainfall season (April-September). It results  $|\mathcal{K}| = 8784$  observations. The locations have been selected among many monitoring locations (red points on Figure 8 ), keeping the elevations above mean sea level between 2 to 540 meters, in order to ensure the spatial stationarity. The data is available freely on the website of Australian meteorology Bureau <http://www.bom.gov.au>. The spatial stationarity and isotropy properties have been investigated for the this data in many papers, for instance see e.g., Bacro et al. (2016), Ahmed et al. (2017) and Abu-Awwad et al. (2019). We shall consider that the data is stationary and isotropic. That leads to construct the corresponding dependence structure directly form the data itself without having to estimate the residuals as in the previous section. Let  $\{X_k(s)\}_{s \in \mathcal{S}, k \in \mathcal{K}}$ ,  $s = 1, \dots, 40, k = 1, \dots, 8784$  be the spatial process representing the rainfall in the East cost of Australia. Adopting the block maxima size as in the previous section, we consider the extreme process:

$$Y_k(s) = \max_{(s, k^*) \in B_{m,k}(s)} X_{k^*}(s)$$

and transform  $Y$  into a unite Fréchet marginals process. The dependence structure of this data will be summarized in a  $40 \times 40 \times 2$  array. The first and second tensor are  $\hat{\chi}_{0,975}(s, t)$  and  $\hat{\hat{\chi}}_{0,975}(s, t)$ ,  $s, t = 1, \dots, 40$ , respectively with threshold  $u = 0.975$ .

### 6.2.2 | Predicting the pattern of the dependence structure of rainfall amount in East Austria.

We shall use same designed CNN in the previous section. The training and validation progress are shown in Figure 9 ,

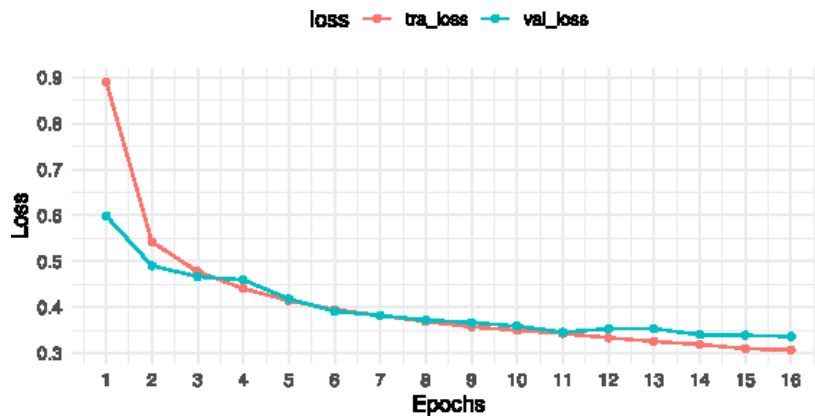


**FIGURE 9** Loss of training and validation recorded for each of the 16 epochs during the training progress.

The validation loss reached the minimum at epoch 16, so the final performance of CNN will be calculated at this epoch. The training and validation recorded loss are 0.307 and 0.336, respectively. The accuracy are 0.889 and 0.875. The loss and

accuracy of the tested data were 0.342 of loss and 0.870 accuracy. Table 4 shows the predicted class for each proposed block maxima size.

**TABLE 4** Predicted class of the Rainfall data for each block maxima size proposed. The dependence structure is classified with the two trained CNN. AD and AI refers to asymptotic dependence and asymptotic independence, respectively.

Block Maxima size	2 classes CNN		3 Classes CNN		
	Probability of AD	Probability of AI	Probability of AD	Probability of AI	Probability of mix
$m = 183$ days	0.020	0.980	0.020	0.980	0.000
$m = 30$ days	0.020	0.980	0.020	0.980	0.000
$m = 15$ days	0.060	0.940	0.063	0.937	0.000
$m = 10$ days	0.271	0.729	0.143	0.808	0.049
$m = 5$ days	0.580	0.420	0.411	0.368	0.221
$m = 3$ days	0.746	0.254	0.000	0.009	0.991
$m = 1$ day	0.946	0.054	0.000	0.001	0.999

The classification procedure shows that the asymptotic independence structure is more suitable for block maxima sizes up to 10 days. This is in accordance with Bacro et al. (2016) where rainfall amount the same region, but for different locations was studied. They concluded that it is not suitable to choose asymptotic dependence models for modeling seasonal maxima. While for block maxima of size  $m = 5$  the prediction is not decisive for the 2-class CNN. For 3 days and daily block maxima, the classifier with 2 classes gives a high probability for asymptotic dependence model. While, CNN with 3 classes, gives different predictions: with high probability a mixture between AD and AI should be chosen. Furthermore, the investigation for the same data has been done in previous works using different block maxima sizes, see Bacro et al. (2016), Ahmed et al. (2017) and Abu-Awwad et al. (2019). They founded that max-mixture models are suitable. This is confirmed by the prediction of CNN with 3 classes.

## 7 | DISCUSSION AND CONCLUSIONS

Since the kind of dependence structures may have influence on the nature of joined extreme events, it is important to devote studies to this matter. Most of the studies deal with modeling extreme events directly by parametrical statistics methods, usually, without preliminary investigation on which pattern of dependence structure would be the most suitable. Moreover, the block maxima size has influence on the dependence structure. In this paper, far from the classical methods, we proposed to exploit the powerfulness of Convolutional Neural Network to investigate the pattern of the dependence structure of the extreme events. Two environmental data (air temperature at two meters over Iraq and rainfall over the East coast of Australia) have been studied in order to classify their dependence structures patterns. The input of the designed CNN are the empirical upper and lower tail

dependence measures  $\hat{\chi}_{0.975}(s, t)$  and  $\hat{\chi}_{0.975}(s, t)$ . The training process has been done on generated data from max-stable stable models, inverse max-stable processes and extreme Gaussian processes, in order to get asymptotic independent models. The data are generated according to fixed coordinates rescaled in  $[0, 1]^2$ . The ability of this model to recognize the pattern of dependence structure has been emphasized in training, validation, testing loss and accuracy.

It is worth mentioning that the sensitivity of the dependence structure class by considering the size of block maxima should be taking into account in the models. Adopting this classification procedure may advise for choosing a reasonable size of block maxima such that the data has a good representation. For instance, for the air temperature event, whatever the block maxima size is chosen, the dependence structure is asymptotic independence. While, for rainfall data, the dependence structure class changed across block size.

## ACKNOWLEDGMENTS

This work was supported by PAUSE operated by Collège de France, and the LABEX MILYON (ANR-10-LABX-0070) of Université de Lyon, within the program “Investissements d’Avenir” (ANR-11-IDEX-0007) operated by the French National Research Agency (ANR).

## References

- Abu-Awwad, A., Maume-Deschamps, V., & Ribereau, P. (2019). Fitting spatial max-mixture processes with unknown extremal dependence class: an exploratory analysis tool. *Test*, 1–44.
- Ahmed, M., Maume-Deschamps, V., Ribereau, P., & Vial, C. (2017). A semi-parametric estimation for max-mixture spatial processes. *arXiv preprint arXiv:1710.08120*.
- Alex, K., Sutskever, L., & Hinton, G. (2012). Imagenet classification with deep convolutional neural networks. In F. Pereira, C. J. C. Burges, L. Bottou, & K. Q. Weinberger (Eds.), *Advances in neural information processing systems 25* (pp. 1097–1105). Curran Associates, Inc. Retrieved from <http://papers.nips.cc/paper/4824-imagenet-classification-with-deep-convolutional-neural-networks.pdf>
- Bacro, J., Gaetan, C., & Toulemonde, G. (2016). A flexible dependence model for spatial extremes. *Journal of Statistical Planning and Inference*, 172, 36–52.
- Bortot, P., Coles, S., & Tawn, J. (2000). The multivariate gaussian tail model: An application to oceanographic data. *Journal of the Royal Statistical Society: Series C (Applied Statistics)*, 49(1), 31–049.
- Brown, B. M., & Resnick, S. I. (1977). Extreme values of independent stochastic processes. *Journal of Applied Probability*,

14(4), 732–739.

- Caterini, A. L., & Chang, D. E. (2018). *Deep neural networks in a mathematical framework*. Springer.
- Coles, S., Heffernan, J., & Tawn, J. (1999). Dependence measures for extreme value analyses. *Extremes*, 2(4), 339–365.
- Coles, S., & Pauli, F. (2002). Models and inference for uncertainty in extremal dependence. *Biometrika*, 89(1), 183–196.
- De Haan, L., & Ferreira, A. (2007). *Extreme value theory: an introduction*. Springer Science & Business Media.
- De Haan, L., et al. (1984). A spectral representation for max-stable processes. *The annals of probability*, 12(4), 1194–1204.
- De Haan, L., Pereira, T. T., et al. (2006). Spatial extremes: Models for the stationary case. *The annals of statistics*, 34(1), 146–168.
- Embrechts, P., Klüppelberg, C., & Mikosch, T. (2013). *Modelling extremal events: for insurance and finance* (Vol. 33). Springer Science & Business Media.
- Fukushima, K. (1980). Neocognitron: A self-organizing neural network model for a mechanism of pattern recognition unaffected by shift in position. *Biological cybernetics*, 36(4), 193–202.
- He, K., Zhang, X., Ren, S., & Sun, J. (2016). Deep residual learning for image recognition. In *Proceedings of the IEEE conference on computer vision and pattern recognition* (pp. 770–778).
- Hooker, J., Duveiller, G., & Cescatti, A. (2018). A global dataset of air temperature derived from satellite remote sensing and weather stations. *Scientific data*, 5(1), 1–11.
- Hubel, D. H., & Wiesel, T. N. (1968). Receptive fields and functional architecture of monkey striate cortex. *The Journal of physiology*, 195(1), 215–243.
- Huser, R. (2020). Eva 2019 data competition on spatio-temporal prediction of red sea surface temperature extremes. *Extremes*, 1–14.
- Kabluchko, Z., Schlather, M., De Haan, L., et al. (2009). Stationary max-stable fields associated to negative definite functions. *The Annals of Probability*, 37(5), 2042–2065.
- Kingma, D., & Ba, J. (2014). Adam: A method for stochastic optimization. *arXiv preprint arXiv:1412.6980*.
- LeCun, Y., Boser, B. E., Denker, J. S., Henderson, D., Howard, R. E., Hubbard, W. E., & Jackel, L. D. (1990). Handwritten digit recognition with a back-propagation network. In *Advances in neural information processing systems* (pp. 396–404).
- Ledford, A., & Tawn, J. A. (1996). Statistics for near independence in multivariate extreme values. *Biometrika*, 83(1), 169–187.
- Lin, Y., Mago, N., Gao, Y., Li, Y., Chiang, Y., Shahabi, C., & Ambite, J. L. (2018). Exploiting spatiotemporal patterns for accurate air quality forecasting using deep learning. In *Proceedings of the 26th ACM SIGSPATIAL international conference on advances in geographic information systems* (pp. 359–368).
- Liu, Y., Racah, E., Correa, J., Khosrowshahi, A., Lavers, D., Kunkel, K., ... others (2016). Application of deep convolutional neural networks for detecting extreme weather in climate datasets. *arXiv preprint arXiv:1605.01156*.

- Opitz, T. (2013). Extremal t processes: Elliptical domain of attraction and a spectral representation. *Journal of Multivariate Analysis*, 122, 409–413.
- Schlather, M. (2002). Models for stationary max-stable random fields. *Extremes*, 5(1), 33–44.
- Schlather, M., & Tawn, J. A. (2003). A dependence measure for multivariate and spatial extreme values: Properties and inference. *Biometrika*, 90(1), 139–156.
- Smith, R. L. (1990). Max-stable processes and spatial extremes. *Unpublished manuscript*, 205.
- Wadsworth, J. L., & Tawn, J. A. (2012). Dependence modelling for spatial extremes. *Biometrika*, 99(2), 253–272.
- Wang, S., Cao, J., & Yu, P. S. (2019). Deep learning for spatio-temporal data mining: A survey. *arXiv preprint arXiv:1906.04928*.
- Xie, S., Girshick, R., Dollár, P., Tu, Z., & He, K. (2017). Aggregated residual transformations for deep neural networks. In *Proceedings of the IEEE conference on computer vision and pattern recognition* (pp. 1492–1500).
- Yamashita, R., Nishio, M., Do, R., & Togashi, K. (2018). Convolutional neural networks: an overview and application in radiology. *Insights into imaging*, 9(4), 611–629.
- Yu, H., Uy, W. I. T., & Dauwels, J. (2016). Modeling spatial extremes via ensemble-of-trees of pairwise copulas. *IEEE Transactions on Signal Processing*, 65(3), 571–586.
- Zhu, Q., Chen, J., Zhu, L., Duan, X., & Liu, Y. (2018). Wind speed prediction with spatio-temporal correlation: A deep learning approach. *Energies*, 11(4), 705.
- Zuo, Z., Shuai, B., Wang, G., Liu, X., Wang, X., Wang, B., & Chen, Y. (2015). Convolutional recurrent neural networks: Learning spatial dependencies for image representation. In *Proceedings of the IEEE conference on computer vision and pattern recognition workshops* (pp. 18–26).

